View metadata, citation and similar papers at core.ac.uk

brought to you by CORE

provided by Elsevier - Publisher Connector

Acta Materialia 103 (2016) 616–623

Contents lists available at ScienceDirect

Acta Materialia

journal homepage: www.elsevier.com/locate/actamat

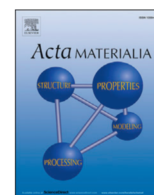

Full length article

High resolution determination of local residual stress gradients in single- and multilayer thin film systems

R. Treml [a], D. Kozic [b], J. Zechner [c], X. Maeder [c], B. Sartory [b], H.-P. Gänser [b], R. Schöngrundner [b], J. Michler [c], R. Brunner [b], D. Kiener [a,*]

[a] Department Materials Physics, Montanuniversität Leoben, Austria
[b] Material Center Leoben Forschung GmbH, Leoben, Austria
[c] Empa, Swiss Federal Laboratories for Materials Science and Technology, Laboratory for Mechanics of Materials and Nanostructures, Thun, Switzerland

ARTICLE INFO

Article history:
Received 27 July 2015
Received in revised form 14 October 2015
Accepted 30 October 2015
Available online 17 November 2015

Keywords:
Residual stress
Ion beam layer removal (ILR)
Multilayer thin films
Physical vapour deposition (PVD)
X-ray diffraction

ABSTRACT

Residual stresses and stress gradients are of great importance in all thin film systems, as they critically influence the structural stability and functionality, and thus the lifetime, of the concerned devices. In this study, an improved ion beam layer removal method is developed to determine the stress distribution in copper- and tungsten-based thin film systems. Cantilevers were prepared from single, bi- and tri-layer systems with an individual layer thickness of 500 nm using focused ion beam machining. Subsequently, residual stress profiles were determined with a depth resolution of 50 nm, employing the ion beam layer removal method. We observe that the evaluated average film stresses correspond to state-of-the-art X-ray diffraction measurements. However, depending on the layer order, different stress profiles with strong stress gradients evolve, and pronounced changes in residual stress occur across an interface within only few grains. These novel findings have profound implications when addressing the interface adhesion, fracture properties and reliability of novel thin film systems, as well as interface dominated materials in general.

© 2015 Acta Materialia Inc. Published by Elsevier Ltd. This is an open access article under the CC BY-NC-ND license (http://creativecommons.org/licenses/by-nc-nd/4.0/).

1. Introduction

Patterned multilayer thin film structures are commonly used in microelectronic applications, simply because single material layers are not able to perform on the same level in terms of required functionality [1]. Notably, besides the primary functionality, the structural stability has to be fulfilled within such patterned multilayer systems as well. In such thin films residual stresses are one of the major challenges to be considered. They can cause damage, fatigue, delamination and cracking of the films, thereby limiting the service life of the whole structure [2]. Components are continually getting smaller, but at the same time new technologies, such as for example the through silicon via (TSV) technology and 3-D integration [3,4], are being developed. Therefore, it is increasingly important to measure residual stresses at the same dimensional scale as that which is used in industrially manufactured devices. With conventional methods such as X-ray diffraction (XRD) or wafer curvature measurements [5–8], the residual stresses in thin films can only be determined globally. Thus, techniques that make a high local resolution for such measurements possible are highly relevant for the modern microelectronics industry. In recent years, several methods to analyse the residual stresses and stress gradients in single and multilayer thin film systems have become available. One way is to perform cross-sectional nanodiffraction experiments [9,10] using finely focused synchrotron radiation at large-scale facilities to determine the stress distribution in thin films in a depth-resolved manner. Another X-ray technique capable of deducing stress gradients proposes measurements at fixed penetration/information depths [11]. Only single layers can be analysed with this method. Another general limitation of X-ray based techniques is the fact that they are only applicable to crystalline materials. A completely different approach suggests micromachined cantilevers where the stress profile is measured through interferometric profilometry [12,13]. Such approaches allow fabrication of many samples by lithographic means, but come at the cost of limited flexibility regarding the material systems that can be processed lithographically. A third group of methods for the local determination of residual stresses comprises incremental focused ion beam (FIB) milling to determine material relaxation due to stress redistribution upon material removal. Different measurement geometries such as slits [4,14,15], pillars [16–19] and micro cantilevers [20,21] are available. These methods are generally applicable to crystalline and amorphous, as well as to textured materials, and provide data from specific positions of a film/sample or local features on a patterned structure. In

* Corresponding author.
E-mail address: daniel.kiener@unileoben.ac.at (D. Kiener).

http://dx.doi.org/10.1016/j.actamat.2015.10.044
1359-6454/© 2015 Acta Materialia Inc. Published by Elsevier Ltd. This is an open access article under the CC BY-NC-ND license (http://creativecommons.org/licenses/by-nc-nd/4.0/).

Table 1
Overview of investigated material systems.

Sample	1st Layer [nm]	2nd Layer [nm]	3rd Layer [nm]
Cu	Cu 483 ± 4	–	–
W–W	W 504 ± 4	W 490 ± 1	–
W–Cu–W	W 486 ± 3	Cu 492 ± 1	W 483 ± 3
Cu–W–Cu BB1[a]	Cu 483 ± 5	W 477 ± 4	Cu 452 ± 2
Cu–W–Cu BB2	Cu 484 ± 4	W 478 ± 1	Cu 474 ± 5

[a] BB . . . Bending Beam.

Table 2
Deposition and material parameters for Cu and W.

Material	Power [W]	Deposition time [s]	Purity [%]	Target diameter [mm]	Target thickness [mm]
Cu	90	4550	99.99	76.20	3.00
W	125	10280	99.95	76.20	3.18

the case of pillars and slits, the deformation field is analysed using digital image correlation. Therefore, a sufficiently structured surface in the region of interest is required. For ring milling of pillars using a simple computation of the stress field, the height h, diameter d and film thickness t should be equal to ensure complete strain relief [17]. For the more general case of d > t additional FEM analysis is necessary to determine the average stress in the film [18]. As outlined by Sebastiani et al. [19], owing to the calculation procedure, the accuracy of the stress values drops significantly for cutting depth values higher than 40% of the desired pillar height. Thus, when aiming at analysing commonly used thin films of only a few 100 nm thickness, extensive FEM analysis is unavoidable to determine residual stresses.

Therefore, in this paper, we demonstrate the determination of residual stresses and stress gradients using micro cantilevers analysed with the ion beam layer removal (ILR) method [20,21], an incremental layer removal method which was further improved and adapted for use in sub-micron multilayer thin film systems. This method has a high depth resolution of 50 nm in the individual sublayers and a lateral resolution within a few µm, with no limitations concerning film thickness. Thin film systems can be analysed analytically, with an error in residual stress values that is independent over the whole film thickness, and without the need for complex computer image analysis.

The technique is applied to determine the residual stresses in copper (Cu) and tungsten (W) based thin film systems. Both materials are of high interest in microelectronics applications in the context of thermal management and electric conductivity, as they show a good combination of high thermal and electrical conductivity for Cu and, in the case of W, a rather low thermal expansion coefficient for a metal, which is only a factor two higher than for Si [1,22]. To demonstrate the capability of the improved ILR-method, we compare the obtained results to standard lab-based X-ray diffraction residual stress measurements and emphasize the importance of pronounced stress gradients at interfaces that are not accessible by standard X-ray diffraction.

2. Experimental

As indicated above, the focus of the present paper was to study Cu and W films, as they are of high importance in the microelectronics industry. We investigated single layers as well as multilayer systems, the latter for different stack configurations, as there should be a difference in film growth depending on the substrate or previous layer, and thus a change in the residual stress profiles.

Four different film systems were systematically investigated. The stack configurations including precise film thicknesses are given in Table 1. We start with a single Cu film of about 500 nm on a silicon substrate. Then a sample consisting of two W layers was investigated to study the influence of an interrupted deposition. Following, a tri-layer sample consisting of W–Cu–W was prepared, to determine the stress distribution in a configuration with a soft interlayer. Finally a Cu–W–Cu sample was deposited to analyse a reversed stack configuration. All samples were deposited at room temperature on a (100) oriented single crystalline Si wafer with a thickness of 525 µm in a Mantis Sputter System (Mantis, Thame, United Kingdom) with an Ar flow of 45 sccm. Direct current sputtering with three different sputtering targets (Cr, Cu and W) was used in the same deposition chamber. Therefore, the vacuum was never broken when changing from one film material to the other. Before putting down the actual layers to be studied, in all cases 10 nm Cr were deposited as seed layer, to stimulate the growth of either Cu or W on the Si wafer. Further deposition and material parameters are given in Table 2. The films consist of globular grains with a grain size ranging from 60 to 70 nm as determined by a line intercept method from scanning electron microscopy (SEM) images (not shown here).

2.1. Sample preparation

In order to determine the residual stress profiles of thin films on a local scale, micro cantilevers were prepared. The material to be studied was extracted from an area in the middle of the wafer to avoid any influence from inhomogeneous film deposition near the wafer edge. The sample was constructed as follows: First, a narrow freestanding fillet (see Fig. 1b) on the sample is prepared using broad beam ion milling [23]. For this preparation step a

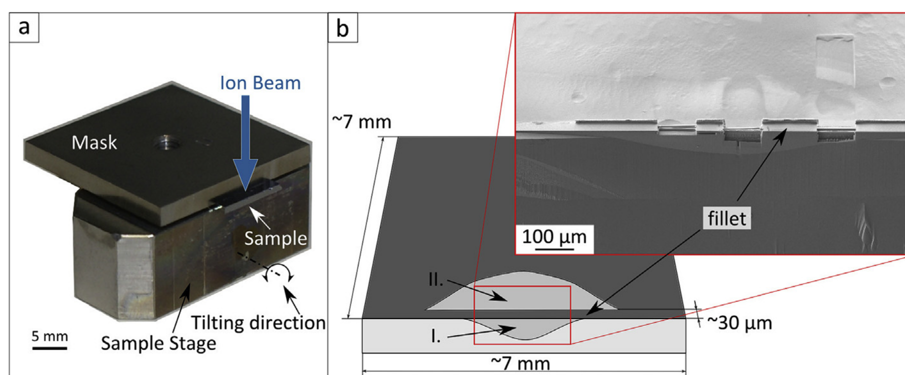

Fig. 1. a) Optical photograph of the sample setup used in the Cross Section Polisher. b) Schematic illustration of the ion-polished lamella with an SEM detail of the actual sample.

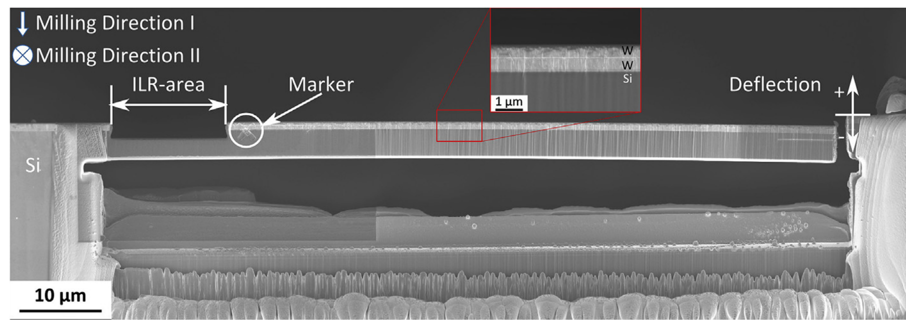

Fig. 2. W–W after the experiment. The ILR-area, the position for the deflection measurement, the marker for stage positioning and the milling directions are denoted.

Hitachi-E3500 Cross Section Polisher (Hitachi, Tokyo, Japan) is used, where low energy Ar ions sputter the material that is not covered by a mask (see Fig. 1a). To protect the film material from ion damage, a lacquer is applied prior to ion milling [24]. In the first milling step (Fig. 1b, label I.) an 80–100 μm wide area is polished off the front edge of the sample to eliminate any deformed material remaining from breaking the wafer. In the second milling step (Fig. 1b, label II.) the sample is rotated by 180° and a narrow area is covered by the mask so that a fillet of 20–30 μm film on the Si substrate remains after the second milling step (see Fig. 1b). Each milling step takes approximately 3 h. The acceleration voltage is set to 6 kV, the discharge voltage to 4 kV and the sample tilting angle around the tilting axis shown in Fig. 1a is ±25° with a tilting speed of 1 rpm. Tilting the sample with respect to the ion beam results in more homogeneous material removal. Advantages of this procedure compared to FIB milling are less ion damage of the sample and a shorter preparation time [24].

The second step concerns the final shaping of the cantilever [20,21]. Here, the sample is loaded into a LEO 1540XB (Zeiss, Oberkochen, Germany) FIB workstation. The front and back are milled from the top (Fig. 2, Milling Direction I) and the bottom from the side (Fig. 2, Milling Direction II). Coarse shaping is done with an ion beam current of 10 nA. For the final polishing step a current of 500 pA is used to minimise Ga^+ ion damage [25]. The final cantilever has a length of approximately 100 μm and a cross-section of approximately 5×4 μm^2.

2.2. Deflection experiments

To determine the stress profile, the cantilever is cut free on one side and the thickness of the film in the rear part of the sample, called ILR-area with a length of approximately 15 μm (Fig. 2), is reduced gradually using the FIB. Thus, the curvature changes in the ILR-area. The rest of the cantilever stays unaltered and acts as an amplifier for this curvature. The cantilever deflection is measured at the tip (Fig. 2). Due to stress redistribution, this deflection changes gradually with each step of thickness reduction [20,21].

In order to provide data with the high spatial resolution needed to determine the residual stress profiles in multilayer thin film systems, the experiments were carried out on an AURIGA-CrossBeam workstation (Zeiss, Oberkochen, Germany) including a self-developed fully automated cutting routine. This routine works as follows: First a marker, in our case a cross (see Figs. 2 and 3D), is cut into the sample near the ILR-area (Milling Direction II). This makes it possible to position the FIB cuts for the thickness reduction in the ILR-area precisely in a later step. Next, a horizontal line for measuring the deflection is milled into the cantilever tip (see Fig. 3, B1 and B2, Milling Direction II). Subsequently, the cantilever is cut free on this side of the beam (Milling Direction II). In the next step, all relevant positions of the sample stage for cutting under a 54° tilting angle and imaging without tilting are stored and tested for proper re-positioning several times to make sure that the stage moving sequence works properly. Subsequently, the cutting window for

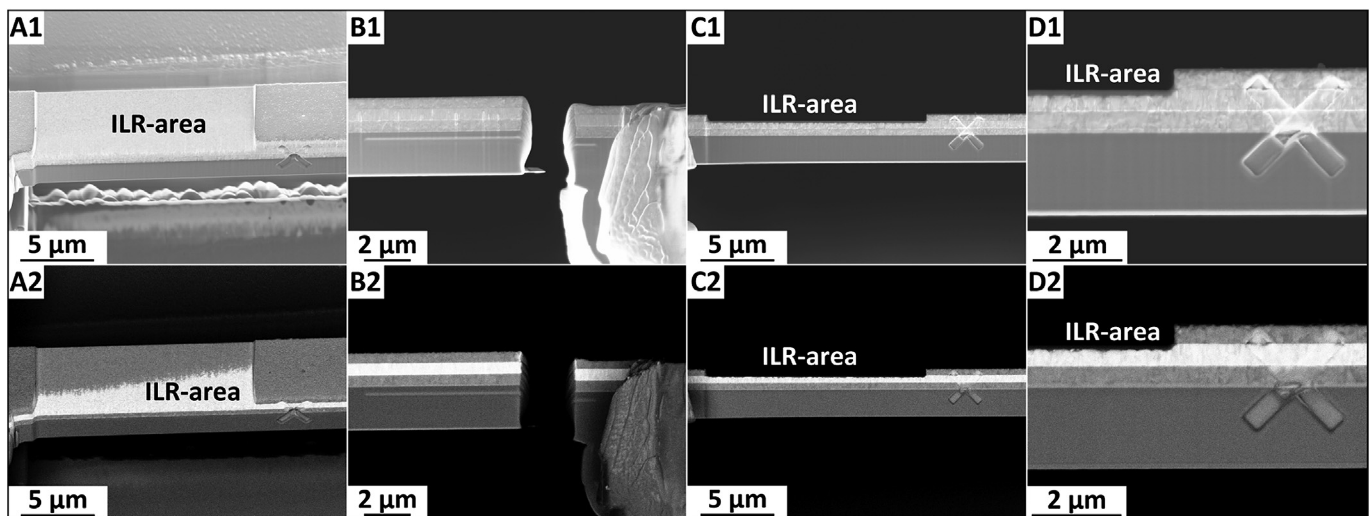

Fig. 3. Individual frames of the SEM image sequence that is collected after each cutting step during the experiment for a Cu–W–Cu sample. A1, B1, C1 and D1 are in-lens SE-images. A2, B2, C2 and D2 are taken with an EsB-detector. A1, A2: ILR-area imaged with a tilting angle of 54° to determine the interface position. B1, B2: Top view of the cantilever tip to measure the deflection. C1, C2: Top view to determine the length of the ILR-area. D1, D2: Enlarged top view of the ILR-area to measure the cutting depth precisely.

material removal in Milling Direction II, the milling current and milling time are prescribed. Then the cutting routine is started, removing 50 nm of material per step. Notably, this is a free parameter that can be set to any length supported by the FIB in use. However, to find a perfect balance between FIB time used and resolution required, we set this parameter to 50 nm, thus roughly matching the grain size and delivering ten data points per film layer. The images of the ILR-area and the cantilever tip, shown in Fig. 3, are taken automatically after each FIB cut with the in-lens secondary electron (SE) and the energy selective back-scattered (EsB) detector. Pictures A are used to determine the exact position of the interface, as described in section 3. The deflection is measured from the line marker in the images B. This view is again recorded after position C and D. This results in three pictures of the same position, allowing us to estimate the statistical error of the deflection measurement. The length of the ILR-area is determined from view C, and the cutting depth from view D. An exemplary quasi *in situ* video is available in the supplementary online material, showing the image sequences taken in views A, B and C during the experiment for a Cu–W–Cu sample, in conjunction with the measured thickness-deflection data. The complete modified ILR procedure without sample alignment to remove approximately 2 μm (film and part of the substrate) including image acquisition takes about 8.5 h. The major part of this time is attributed to re-positioning of the stage, the image recording and drift equalization, rather than for FIB cutting. Therefore, processing time could be substantially reduced by using fast settling piezo stages.

Supplementary data related to this article can be found online at http://dx.doi.org/10.1016/j.actamat.2015.10.044.

2.3. XRD measurements

For complementary determination of the in-plane residual stresses, XRD measurements are employed using the $\sin^2\psi$-method [26,27]. As there is a linear relationship between lattice spacing and $\sin^2\psi$, the stress is calculated from the measured slope, taking into account the elastic properties of the material. The measurement was performed on a Bruker D8 diffractometer equipped with an Eulerian cradle, a Göbel mirror with a point focus of 1 mm and a Cu radiation source ($\lambda = 1.5406$ Å) operating at 40 kV and 40 mA. The strain was measured on the W (321) peak at $2\theta = 131°$ and on the Cu (311) peak at $2\theta = 90°$. Both peak positions were measured at ψ increments of 5°, from 0 to 45° from the sample surface. A uniaxial in-plane stress is assumed in each of the layers, but for statistical reason, the strain was measured in two perpendicular in-plane directions for each peak and ψ angle positions. The in-plane macro-stress was calculated using a Young's modulus of E = 115 GPa and a Poisson's ratio of $\nu = 0.36$ for Cu (311), and E = 411 GPa, $\nu = 0.28$ for W (321) [28].

3. Analysis and results

3.1. ILR stress analysis

The positioning of the sample in the FIB is crucial for the high resolution measurements. The task was to align the interfaces parallel to the ion beam. Therefore, the sample has to be tilted slightly more/less than 54° to compensate for the taper of the ion beam. However, a finite small misalignment will typically remain, which is the reason that the transition between the two films is not completely sharp. Therefore, it is necessary to define an image where the interface is set to assign the elastic properties. Fig. 3A illustrates this circumstance using a Cu–W-interface as an example, with Cu being the darker material. The convention used to determine the interface position is that half of the cut surface area is still covered with Cu, while in the other half W is already visible, as seen in Fig. 3

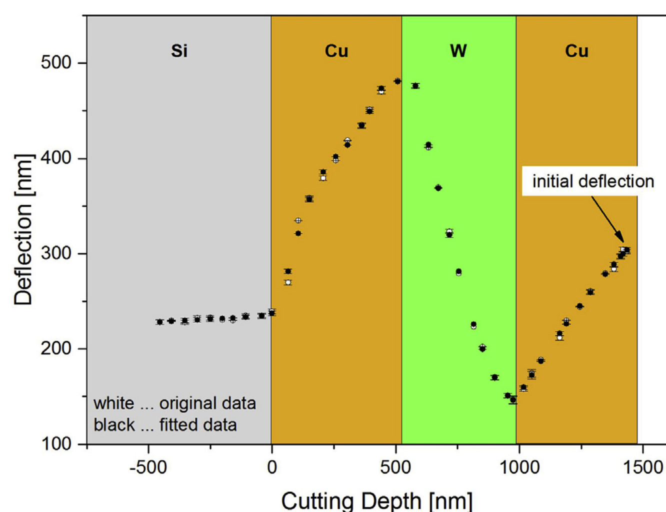

Fig. 4. Original (white dots) and fitted (black dots) deflection profile of a Cu–W–Cu cantilever, showing gradual changes across the different layers. Reducing deflections are observed in the Cu layers, while they increase in the W layer.

A2. To analyse the data, the corresponding deflections and remaining film thickness are determined from the images in views B and D of Fig. 3. As mentioned before, the cantilever tip is imaged three times. Thus, three deflection values are determined from the images, and the arithmetic mean value and the standard deviation are calculated from these measurements. More images for better statistics would be preferable, however, a trade-off with respect to instrument use and surface contamination was made. To eliminate possible runaway values, the measured deflections and film thicknesses were split up in sections, one for each layer, and fitted by higher order polynomial functions. An exemplary comparison between a fitted (black dots) and unfitted (white dots) deflection profile is shown in Fig. 4 for a Cu–W–Cu sample. The evolution of the deflection profile is described in the direction of material removal (from right to left), as the deflection changes due to the removal of film material. The initial deflection of the beam (indicated by an arrow) is 304 ± 2 nm, which decreases to a deflection of 147 ± 4 nm as the whole 500 nm of Cu are removed. Once the material removal takes place in the W layer, the change in deflection reverses and increases up to 481 ± 2 nm. This changes again when removing the second Cu layer. After removing all Cu, the deflection at the interface between Cu and Si is 237 ± 2 nm and remains more or less constant as the thickness of the Si is reduced by approximately 500 nm. This finite deflection of the beam originates from the curvature induced by the residual stresses stored in the remaining film on the cantilever, outside of the ILR-area.

An analytical solution to calculate the residual stress profiles is realized in a script [29] in the computer algebra system Maple™ (Maplesoft, Waterloo, Canada). The calculation relies on the Euler-Bernoulli theory for bending beams, as already described in Refs. [20,21]. Input parameters for the calculation are the geometry data from the experiment, the elastic material properties (Table 3), and the thickness of the removed layers with the corresponding deflections. After providing this initial input, every following sequence

Table 3
Material properties for stress calculation [30–32].

Material	Young's modulus [GPa]	Poisson's ration [–]
Si	170	0.28
Cu	130	0.34
W	411	0.28

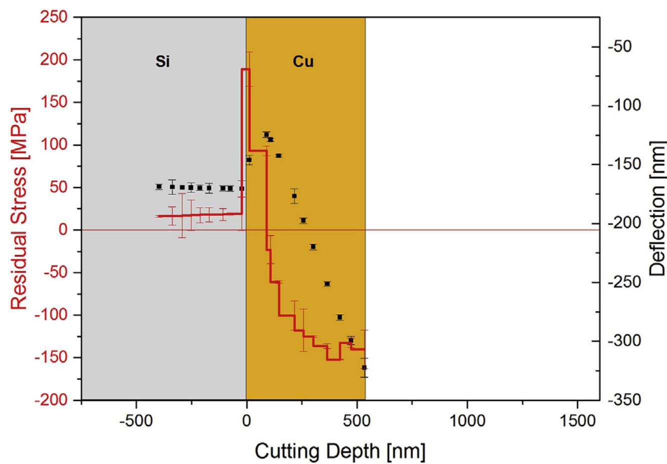

Fig. 5. Deflection and residual stress profile of a 500 nm Cu film on Si substrate as a function of the cutting depth.

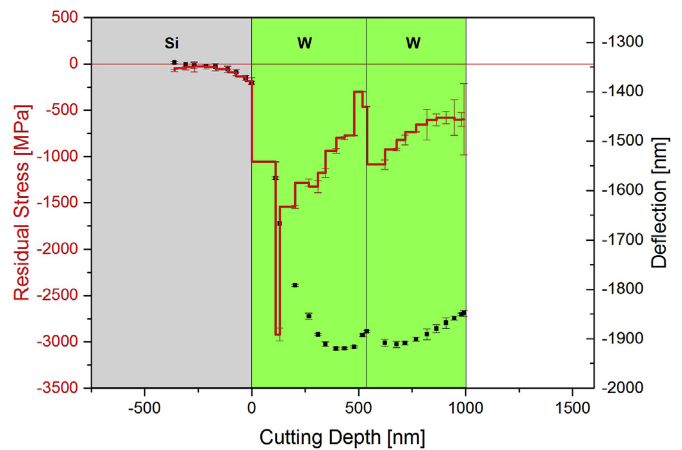

Fig. 6. Deflection and residual stress profile of a W–W bilayer on Si.

in the script is performed automatically. In an iterative loop the layers are re-deposited step by step under the assumption that the substrate is initially straight and stress-free. The stress for each layer is calculated from the force and momentum balance, depending on the stress determined for the previous layers and the curvature for the current layer. Finally, the residual stress distribution is returned. As mentioned before, the stress distribution is determined from the fitted data, the error bars correspond to plus/minus one time the standard deviation.

Further details on the calculation procedure are given in Ref. [29], and a detailed assessment of possible influences of boundary conditions, *e.g.* stress relaxation due to finite beam width or deformation of the beam fixation, was performed previously to assure a robust analytical routine delivering reliable data [21].

3.2. Stress results

First, the single Cu layer is described, as this is the simplest case with no additional interfaces present. In Fig. 5, the experimental deflection (black dots) and computed residual stress profile (red line) are depicted. The stress profiles in the results sections are described in the growth direction (from left to right), as the stresses build up during growth. We see a more or less constant deflection in the Si with a value of –171 ± 7 nm at the interface to Cu caused by the remaining film on the cantilever. In the first 90 nm of the Cu film, the deflection decreases to –125 ± 2 nm and increases to –322 ± 8 nm at the surface. In the Si substrate, the residual stress remains approximately constant at 17 ± 17 MPa. At the interface between Cu and Si the tensile stress reaches a maximum of 189 ± 20 MPa. The change in sign of the stress values occurs at the turning point of the deflection at a thickness of 90 nm and decreases further to –140 ± 22 MPa compressive residual stress at the surface.

For the following samples, only the stress values are addressed, as these are the prime interest for the remainder of the work.

The next sample consists of two W layers, with a holding time of 4550 s in between the two W depositions, which would correspond to the deposition time of a 500 nm Cu layer, see Table 2. In Fig. 6, the deflection (black dots) and residual stress (red line) profiles of the W–W bilayer cantilever are depicted. In the Si substrate, the residual stress remains approximately constant at –27 ± 27 MPa. For the first W layer, the residual stress profile shows a U-shape with a runaway value at 130 nm W film thickness. At the W–W interface the residual compressive stress jumps from –462 ± 3 MPa to –1088 ± 52 MPa and reaches a value of –599 ± 385 MPa at the surface.

For the following sample the influence of a Cu interlayer between the two W layers is investigated. In Fig. 7 the deflection (black dots) and residual stress (red line) profiles of such a W–Cu–W multilayer cantilever are presented.

Again, as one would expect, the stress in Si is almost zero and constant. In the first W layer the stress profile shows a U-shape with a minimum value of –1501 ± 23 MPa. At the interface to Cu the stress jumps from a compressive stress of –679 ± 27 MPa to 273 ± 82 MPa tensile stress. In the Cu layer only a slight increase in residual stress up to 421 ± 46 MPa is measured. When entering the second W layer the stress changes to compressive within less than 100 nm and decreases to –588 ± 2 MPa at the surface.

Next, two samples with slightly different beam heights (BB1 = 3.3 μm, BB2 = 4.3 μm), but both consisting of a W layer enclosed by two copper layers are considered to investigate the change in the residual stress profile due to the altered deposition sequence, as well as the general reproducibility of the method. In Fig. 8, the deflection (black) and residual stress (red) profiles of the two Cu–W–Cu multilayer cantilevers are depicted.

For both samples the profile in the Si substrate remains constant at zero stress. In the first Cu layer the stress is tensile and stays almost constant at around 200 MPa for both samples. In the W layer the stress profiles are U-shaped with minimum compressive stress values of –641 ± 15 MPa (BB1) and –438 ± 2 MPa (BB2). Again

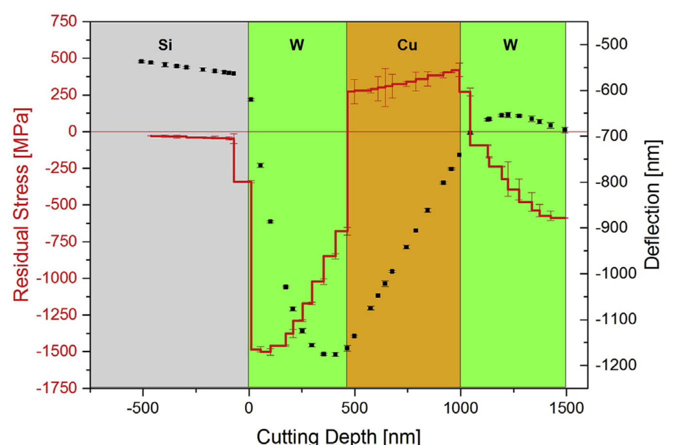

Fig. 7. Deflection and residual stress profile of a W–Cu–W multilayer on a Si substrate.

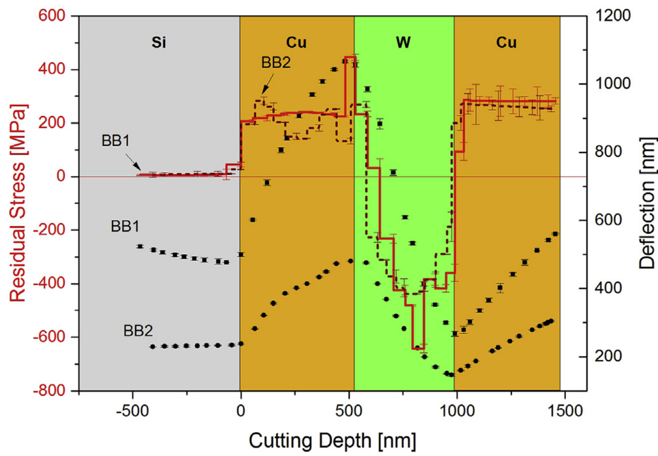

Fig. 8. Deflection and residual stress profile of two samples of a Cu–W–Cu multilayer on Si substrate as a function of the film thickness.

pronounced jumps in residual stress are observed at both Cu/W interfaces. The second Cu layer shows tensile stresses with values of 282 ± 12 MPa (BB1) and 253 ± 11 MPa (BB2) at the surface, respectively.

For a later comparison of our depth-resolved residual stresses to XRD measurements, the linear average film stresses of each layer were calculated for all tested systems (Table 4).

3.3. Results XRD

The XRD measurements were performed along two directions to exclude possible anisotropy. They show tensile stresses for the Cu layer in the tri-layer samples and compressive stress for the single Cu layer. The W layers exhibit compressive stress. The precise values are given in Table 5 for 0° and 90°, respectively. The difference between the two directions is within the experimental scatter, thus confirming homogenous in-plane properties.

While the sign of the stresses is consistent for all layers between the two techniques, there are some differences in the absolute stress values, in particular for the W films. This is attributed to the penetration depth of the XRD signal, which is discussed below.

Table 4
Averaged residual layer stress determined with ILR-method.

Sample	1st Layer [MPa]	2nd Layer [MPa]	3rd Layer [MPa]
Cu	Cu –70	–	–
W–W	W –1141	W –755	–
W–Cu–W	W –1060	Cu +336	W –315
Cu–W–Cu BB1	Cu +206	W –211	Cu +268
Cu–W–Cu BB2	Cu +197	W –252	Cu +257

Table 5
Residual stresses determined by XRD measurements.

Sample	Cu [MPa]	W [MPa]
Cu	–73.6 ± 4.3	
W–Cu–W	162 ± 59 (0°)	–509 ± 14 (0°)
	214 ± 36 (90°)	–548 ± 20 (90°)
Cu–W–Cu	179 ± 30 (0°)	–387 ± 37 (0°)
	158 ± 29 (90°)	–341 ± 21 (90°)

4. Discussion

According to thin film data from literature, Cu films with a thickness of a few 100 nm show tensile residual stresses ranging from 100 to 500 MPa [33–35]. For W films with a layer thickness of only a few nm, compressive stresses ranging from –3 to –8 GPa are reported [35,36]. Thicker W layers of 100 nm exhibit lower compressive stresses of around –2 GPa [37], as there is a well-known trend to lower stresses for thicker films [38,39]. In these cases, the global residual stresses were determined either by wafer curvature [34] or XRD [33,35–37]. In the present case, the 500 nm W layers exhibit compressive stresses ranging from –200 to –1100 MPa, which is well within the range of literature reported in Refs. [35–37]. This trend to lower average stress for increasing film thickness can be explained by the fact that the stress is highest at the interface due to the growth process (impinging sputter atoms) and the misfit between Si substrate and film. Furthermore, growth defects near the interface contribute less to the average stress for thicker films [39]. This is also well reflected in the local stress gradient in this work, where the residual stress decreases with increasing distance from the interface (see e.g. Figs. 6 and 7).

Before discussing the stress gradients in more detail, we compare the average stress values in each layer to state-of-the-art XRD measurements. To this end, the average stresses in each layer evaluated using the two methods are plotted side by side in Fig. 9. Additionally, data bars indicate the maximum and minimum stress of each layer determined by the ILR method. Looking at the single Cu layer, the ILR and XRD results agree well. At first glance, compressive stresses might seem uncommon, as the single Cu layer is the only sample in this series showing compressive stresses. However, this sample was studied in the as-received condition, so these compressive stresses might stem from atomic shot peening during deposition [38,40]. A single thermal cycle would anneal defects and drive the Cu towards the tensile stress regime [41]. Additional layer deposition on top of the first Cu layer can also cause a local temperature rise due to the impinging atoms, thereby explaining why the tri-layer samples exhibit tensile residual stresses in the Cu layers. Moreover, for discussing the tri-layer samples, the attenuation of the X-ray beam has to be taken into account when comparing the obtained values. Due to its higher atomic weight, W absorbs the X-ray beam stronger than Cu. When the stack is composed of W–Cu–W (500 nm thickness each), the first W layer absorbs about 30% of the X-ray beam intensity, and the second one about 22%, counting an incident angle of 65.5° (W (321) peak), both way in and out. The total absorption of the stack is about 45% of the beam intensity.

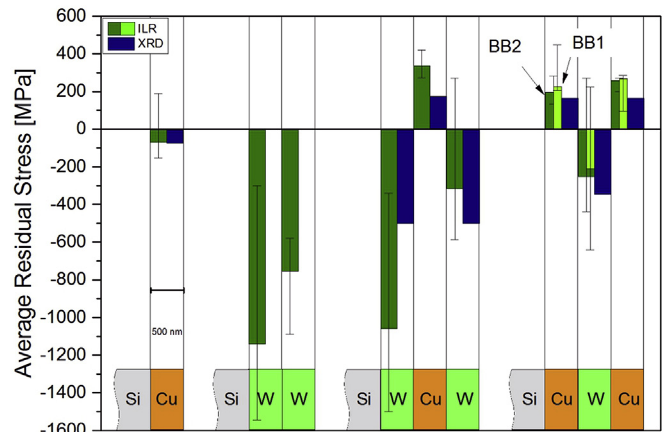

Fig. 9. Comparison of average film stresses determined by the ILR-method and XRD for the different film systems. The data bars indicate the minimum and maximum layer stresses from the ILR measurement.

Therefore, the X-ray stress measurements give values close to mean values for the W and the Cu layer, but with a little more pronounced influence from the first layer. When the stack is composed of Cu–W–Cu (500 nm thickness each), the first Cu layer absorbs about 7% of the X-ray intensity and the second one about 5% (45° incident angle, Cu (311) peak, both way in and out). Again, the first layer will contribute somewhat more to the peak intensity.

As shown in Figs. 7 and 8, for the two cases where Cu grows directly on W (Cu–W–Cu 3rd layer and W–Cu–W 2nd layer), tensile stresses of 250–350 MPa evolve in the Cu. The same holds true for the cases where W is deposited on Cu (Cu–W–Cu 2nd layer and W–Cu–W 3rd layer), where compressive average stresses with a comparable magnitude between −200 and −300 MPa are measured in the W layer. If W grows on the Si wafer instead (W–W 1st layer and W–Cu–W 1st layer), significantly higher compressive stresses of approximately −1100 MPa are built up (see Figs. 6 and 7). Thus, we see that the stress evolution in the individual layers is strongly dependent on the combination of materials that are in contact [34], an information that would be challenging to acquire from bulk methods.

Before discussing the details of the stress gradients, it is seminal to consider the repeatability of the experiments. The two Cu–W–Cu samples (BB1 and BB2) show a difference in average stress values of about 10% (Table 4 and Fig. 9), which is quite satisfying for such miniaturised experiments. This difference could as well be a result of fluctuations in the local stress between neighbouring grains. Such variations between individual grains were reported, for example, by Spolenak et al. [42] for Al 0.5 wt % Cu thin films, where the authors reported even higher deviations in residual stress of 40% between individual grains using micro-Laue diffraction. However, a more detailed assessment of the variations does not appear feasible with the current data, as the differences are presumably within the experimental error.

Nevertheless, these considerations point towards a design criterion for such experiments. While reducing the ILR length would further increase the lateral resolution, it would also render the method more prone to such variations on a grain-to-grain level. On the contrary, increasing the ILR length would further minimize such microstructural effects. This is, however, limited by our ability to FIB mill 50 nm segments of a certain curvature rather than straight segments, which would be required to account for the curvature of the ILR area. Notably, a reduction of the milling segment height on the expense of more FIB time is easily doable. However, if for example only 10 nm of material were to be removed per step, it remains questionable whether the FIB damage [25] could influence the determined material properties.

The majority of films studied in the current paper exhibit pronounced stress gradients. This is a known phenomenon reported several times in the literature for different materials, for example for Ni films [11,20], CrN films [16,43] and TiN films [44]. However, this information was previously accessed in a rather tedious manner, for example by depositing several different thicknesses of the same film and determining the residual stress for each film thickness [39]. For the Cu and the W–W samples, it is evident that the growth process influences the evolution of the stress profile. For the first few grains (they correspond in diameter to the individually removed layers) in the two W layers the shape of the stress profile is different, but then they are in good agreement. It is also evident, that the interrupted deposition has an influence on the deflection profile, and thus on the residual stress profile, over a few grains in both W layers (Fig. 6). Looking at the Cu sample, the stress is tensile for approximately 100 nm and then changes to compressive stress. These findings can be correlated to the growth process of the film, which changes within the first few grains of each layer and is highly sensitive to the deposition parameters [43]. Notably, our experiments are well suited to pick up these changes that occur during film growth. For the samples W–Cu–W (Fig. 7) and Cu–W–Cu BB1 and BB2 (Fig. 8) the tensile stress in the Cu layer is almost constant. However, the stress in the W layers shows pronounced stress gradients. Cu is the much softer material, and it is assumed that stresses can relax and average over the film thickness by local plastic deformation during film growth. W, on the contrary, is the much stiffer material and has a smaller lattice spacing (316 pm) [45] than Cu (361 pm) [46], thus W must expand to fit onto the Cu lattice. Therefore, the compressive stress in W is reduced when approaching the Cu interface.

Finally, it is worth mentioning that the jumps in stress at the interfaces between Cu and W appear to be 510 MPa from average X-ray measurements, while we find changes of 450 MPa over a depth of ~100 nm for Cu–W–Cu BB1, for example. Such information was so far barely accessible, but is important when attempting, for example, to study interface decohesion, film delamination, or fracture properties of such systems experimentally, or to implement it numerically.

5. Conclusion and outlook

The improved ILR-method used in the present study allows for a rapid and precise determination of the residual stress distribution in multilayer thin film systems with a depth resolution of 50 nm and on a lateral scale of only few µm, facilitated by fully automated cutting routines and analysis. A further increase in resolution to few nm is limited by the increasing FIB time and the fact that the first few nm of material is damaged by the FIB. Residual stresses can be routinely measured, even for low values in the range of a few MPa, and are found in good agreement with global XRD measurements for films without pronounced gradients. However, we do note pronounced stress gradients within our films and in particular across interfaces. With the ILR-method it is easily possible to determine these stress gradients on the length scale of the film microstructure, showing that the most severe changes occur within only a few grains. Access to this information is of great importance, as the stress and the stress gradient at the interface influence, for example, the crack initiation, film fracture toughness, crack path, interface delamination, etc. For such highly localised events, considerations using an average stress value determined with conventional methods can be quite misleading. Knowledge of local stress gradients is also important for the design and further improvement of novel multilayer structures or gradient materials, which can be readily studied with the methods developed in this work.

Acknowledgement

Financial support by the Austrian Federal Government (837900) (in particular from the Bundesministerium für Verkehr, Innovation und Technologie and the Bundesministerium für Wissenschaft, Forschung und Wirtschaft) represented by Österreichische Forschungsförderungsgesellschaft mbH and the Styrian and the Tyrolean Provincial Government, represented by Steirische Wirtschaftsförderungsgesellschaft mbH and Standortagentur Tirol, within the framework of the COMET Funding Programme is gratefully acknowledged.

References

[1] A. Luedtke, Thermal management materials for high-performance applications, Adv. Eng. Mater. 6 (2004) 142–144.
[2] G. Janssen, Stress and strain in polycrystalline thin films, Thin Solid Films 515 (2007) 6654–6664.
[3] J.H. Lau, Overview and outlook of through-silicon via (TSV) and 3D integrations, Microelectron. Int. 28 (2011) 8–22.
[4] D. Vogel, E. Auerswald, J. Auersperg, P. Bayat, R. Rodriguez, D. Zahn, S. Rzepka, B. Michel, Stress analyses of high spatial resolution on TSV and BEoL structures, Microelectron. Reliab. 54 (2014) 1963–1968.

[5] I. Noyan, J. Cohen, Residual Stress: Measurement by Diffraction and Interpretation, Springer, 1987.
[6] V. Hauk, Structural and Residual Stress Analysis by Nondestructive Methods, Elsevier, 1997.
[7] L.B. Freund, S. Suresh, Thin Film Materials, Cambridge University Press, Cambridge, 2003.
[8] P.A. Flinn, D.S. Gardner, W.D. Nix, Measurement and interpretation of stress in aluminum-based metallization as a function of thermal history, IEEE Trans. Electron Device ED 34 (1987) 689–699.
[9] J. Keckes, M. Bartosik, R. Daniel, C. Mitterer, G. Maier, W. Ecker, J. Vila-Comamala, C. David, S. Schoeder, M. Burghammer, X-ray nanodiffraction reveals strain and microstructure evolution in nanocrystalline thin films, Scr. Mater. 67 (2012) 748–751.
[10] S. Kurz, S. Meka, N. Schell, W. Ecker, J. Keckes, E. Mittemeijer, Residual stress and microstructure depth gradients in nitrided iron-based alloys revealed by dynamical cross-sectional transmission X-ray microdiffraction, Acta Mater. 87 (2015) 100–110.
[11] A. Kumar, U. Welzel, E. Mittemeijer, A method for the non-destructive analysis of gradients of mechanical stresses by X-ray diffraction measurements at fixed penetration/information depths, J. Appl. Crystallogr. 39 (2006) 633–646.
[12] W. Fang, J.A. Wickert, Determining mean and gradient residual stresses in thin films using micromachined cantilevers, J. Micromech. Microeng 6 (1996) 301–309.
[13] Y. Zhang, Y.-P. Zhao, An effective method of determining the residual stress gradients in a micro-cantilever, Microsyst. Technol. 12 (2006) 357–364.
[14] K.J. Kang, N. Yao, M.Y. He, A.G. Evans, A method for in situ measurement of the residual stress in thin films by using the focused ion beam,, Thin Solid Films 443 (2003) 71–77.
[15] C. Mansilla, D. Martínez-Martínez, V. Ocelík, J.T.M. De Hosson, On the determination of local residual stress gradients by the slit milling method, J. Mater. Sci. 50 (2015) 3646–3655.
[16] E. Bemporad, M. Brisotto, L.E. Depero, M. Gelfi, A.M. Korsunsky, A.J.G. Lunt, M. Sebastiani, A critical comparison between XRD and FIB residual stress measurement techniques in thin films, Thin Solid Films 572 (2014) 224–231.
[17] A.M. Korsunsky, M. Sebastiani, E. Bemporad, Focused ion beam ring drilling for residual stress evaluation, Mater. Lett. 63 (2009) 1961–1963.
[18] X. Song, K.B. Yeap, J. Zhu, J. Belnoue, M. Sebastiani, E. Bemporad, K. Zeng, A.M. Korsunksky, Residual stress measurement in thin films at sub-micron scale using focused ion beam milling and imaging, Thin Solid Films 520 (2012) 2073–2076.
[19] M. Sebastiani, C. Eberl, E. Bemporad, G.M. Pharr, Depth-resolved residual stress analysis of thin film coatings by a new FIB-DIC method, Mater. Sci. Eng. A 528 (2011) 7901–7908.
[20] S. Massl, J. Keckes, R. Pippan, A direct method of determining complex depth profiles of residual stresses in thin films on a nanoscale, Acta Mater. 55 (2007) 4835–4844.
[21] R. Schöngrundner, R. Treml, T. Antretter, D. Kozic, W. Ecker, D. Kiener, R. Brunner, Critical assessment of the determination of residual stress profiles in thin films by means of the ion beam layer removal method, Thin Solid Films 564 (2014) 321–330.
[22] S. Yoo, M. Krupashankara, T. Sudarshan, R. Dowding, Ultrahigh pressure consolidation (UHPC) of W-Cu composites, Mater. Sci. Technol. 14 (1998) 170–174.
[23] S. Wurster, C. Motz, M. Jenko, R. Pippan, Micrometer-sized specimen preparation based on ion slicing technique, Adv. Eng. Mater. 12 (2010) 61–64.
[24] S. Wurster, R. Treml, R. Fritz, M.W. Kapp, E. Langs, M. Alfreider, C. Ruhs, P.J. Imrich, G. Felber, D. Kiener, Novel methods for the site specific preparation of micromechanical structures, Pract. Metallogr. 52 (2015) 131–146.
[25] D. Kiener, C. Motz, M. Rester, M. Jenko, G. Dehm, FIB damage of Cu and possible consequences for miniaturized mechanical tests, Mater. Sci. Eng. A 459 (2007) 262–272.
[26] B. Cullity, S.R. Stock, Elements of X-Ray Diffraction, second ed., Addison-Wesley, Reading, Massachusetts, 1980.
[27] T.J. Vink, M. Somers, J. Daams, A. Dirks, Stress, strain, and microstructure of sputter-deposited Mo thin films, J. Appl. Phys. 70 (1991) 4301–4308.
[28] A.C. Vermeulen, X-ray elastic constants database (XECs), JCPDS-international centre for diffraction data, Adv. X-ray Anal. 44 (2001) 128–133.
[29] D. Kozic, R. Treml, R. Schöngrundner, R. Brunner, D. Kiener, T. Antretter, H.-P. Gänser, Evaluation of the residual stress distribution in thin films by means of the ion beam layer removal method, in: 15th International Conference on Thermal, Mechanical and Multi-physics Simulation and Experiments in Microelectronics and Microsystems, EuroSimE 2014, 2014.
[30] M.A. Hopcroft, W.D. Nix, T.W. Kenny, What is the Young's modulus of silicon, J. Microelectromech. Syst. 19 (2) (2010) 229–238.
[31] P.G. Sanders, J.A. Eastman, J.R. Weertman, Elastic and tensile behavior of nanocrystalline copper and palladium, Acta Mater. 45 (10) (1997) 4019–4025.
[32] E. Harry, A. Rouzaud, M. Ignat, P. Juliet, Mechanical properties of W and W(C) thin films: Young's modulus, fracture toughness and adhesion, Thin Solid Films 332 (1998) 195–201.
[33] T. Hanabusa, K. Kusaka, O. Sakata, Residual stress and thermal stress observation in thin copper films, Thin Solid Films 459 (2004) 245–248.
[34] G. Dehm, T.J. Balk, H. Edongué, E. Arzt, Small-scale plasticity in thin Cu and Al films, Microelectron. Eng. 70 (2003) 412–424.
[35] S. Djaziri, P.-O. Renault, E. Le Bourhis, P. Goudeau, D. Faurie, G. Geandier, C. Mocuta, D. Thiaudière, Comparative study of the mechanical properties of nanostructured thin films on stretchable substrates, J. Appl. Phys. 116 (2014) 093504.
[36] B. Girault, D. Eyidi, T. Chauveau, D. Babonneau, P.-O. Renault, E. Le Bourhis, P. Goudeau, Copper coverage effect on tungsten crystallites texture development in W/Cu nanocomposite thin films, J. Appl. Phys. 109 (2011) 014305.
[37] G.K. Rane, S. Menzel, T. Gemming, J. Eckert, Microstructure, electrical resistivity and stresses in sputter deposited W and Mo films and the influence of the interface on bilayer properties, Thin Solid Films 571 (2014) 1–8.
[38] G.C.A.M. Janssen, J.-D. Kamminga, Stress in hard metal films, Appl. Phys. Lett. 85 (2004) 3086–3088.
[39] H. Köstenbauer, G.A. Fontalvo, M. Kapp, J. Keckes, C. Mitterer, Annealing of intrinsic stresses in sputtered TiN films: The role of thickness-dependent gradients of point defect density, Surf. Coat. Technol. 201 (2007) 4777–4780.
[40] B. Okolo, P. Lamparter, U. Welzel, T. Wagner, E.J. Mittemeijer, Changes in stress and microstructure in sputter deposited copper films due to substrate surface effects, Mater. Sci. Forum 404–407 (2002) 691–696.
[41] S.-J. Hwang, Y.-C. Joo, J. Koike, Stress relaxation during isothermal annealing in electroplated Cu films, Thin Solid Films 516 (2008) 7588–7594.
[42] R. Spolenak, W.L. Brown, N. Tamura, A.A. MacDowell, R.S. Celestre, H.A. Padmore, B. Valek, J.C. Bravman, T. Marieb, H. Fujimoto, B.W. Batterman, J.R. Patel, Local plasticity of Al thin films as revealed by X-Ray microdiffraction, Phys. Rev. Lett. 90 (2003) 096102.
[43] R. Daniel, J. Keckes, I. Matko, M. Burghammer, C. Mitterer, Origins of microstructure and stress gradients in nanocrystalline thin films: the role of growth parameters and self-organization,, Acta Mater. 61 (2013) 6255–6266.
[44] R. Machunze, G.C.A.M. Janssen, Stress gradients in titanium nitride thin films, Surf. Coat. Technol. 203 (2008) 550–553.
[45] W.P. Davey, The lattice parameter and density of pure tungsten, Phys. Rev. 26 (1925) 736–738.
[46] J.R. Davis, ASM speciality handbook: copper and copper alloys, ASM Int. (2001) 446.